Design Study for the JET Diagnostic System: "Quasi-Continuous Laser Scattering[++)]"

Part II

Extension to Spatial Scan

H.Röhr, K.-H. Steuer
K.Hirsch[+)], H.Salzmann[+)]

IPP III/66
IPF 81/3

January 1981

MAX-PLANCK-INSTITUT FÜR PLASMAPHYSIK

8046 GARCHING BEI MÜNCHEN

MAX-PLANCK-INSTITUT FÜR PLASMAPHYSIK

GARCHING BEI MÜNCHEN

Design Study for the JET Diagnostic System: "Quasi-Continuous Laser Scattering[++)]"

Part II

Extension to Spatial Scan

H.Röhr, K.-H. Steuer
K.Hirsch[+)], H.Salzmann[+)]

IPP III/66 January 1981
IPF 81/3

[+)] Institut für Plasmaforschung
der Universität Stuttgart

[++)] This work was done under article 14
of JET Statutes (contract Number B-GI-402)

Die nachstehende Arbeit wurde im Rahmen des Vertrages zwischen dem Max-Planck-Institut für Plasmaphysik und der Europäischen Atomgemeinschaft über die Zusammenarbeit auf dem Gebiete der Plasmaphysik durchgeführt.

Abstract

This report is an update of the design study available as report IPP III/55 or IPF 80-2. Recent improvements in detector performance and calibration techniques are presented and a possible high repetition rate Nd:YAG laser system is described which promises high flexibility of operation and reliability. Further, the collection optics is now designed to obtain a spatial profile with each laser pulse.

Results from a pilot experiment on ASDEX using a single pulse Nd^{3+}:Glass laser and avalanche photodiodes are presented and discussed.

Contents

1) High repetition rate Nd^{3+}:YAG lasers

1a) Status of the Nd^{3+}:YAG laser for ASDEX

JK Lasers has a contract with IPP to deliver a YAG laser system providing 1 J in a single polarization at repetition rate up to 100 Hz for at least a 1 second period. This laser would allow to measure electron density and temperature in a 90^{o} scattering experiment at ASDEX within an error of less than 10 % up to 100 times per sec.. The development of the Nd^{3+}:YAG laser system to meet the required specification has been divided into three phases, i.e.

1) the demonstration of a prototype system meeting the minimum required specification of 50 pulses/sec with 1 Joule energy per pulse
2) the evaluation of options for reducing the system beam divergence
3) extension to a system of 100 Hz.

In Nov. 1980 JK Lasers has met the required specification for 50 Hz operation. This laser consists of an oscillator and two amplifiers with 3 "x 1/4" Nd:YAG rods throughout. A Pockels cell between parallel Glan type polarizers was used as interstage isolator between the amplifiers. The 1 J/pulse output is maintained with $\pm$ 1 % stability over the whole period of operation. It is encouraging that this system can be operated for at least 2 seconds. Best results were obtained with a 1 second warm-up period before Q-switching.

Beam divergence measurements showed that 90 % of the energy of the first pulse and about 75 % of the 50th pulse is contained within a 5.5 mrad cone.

With regard to phase 2 JK Lasers is testing a low divergence oscillator working in the TEM_{oo} - mode followed by 3 amplifiers to reduce the overall divergence by a factor of at least 3.

JK Lasers believes that they have solved the basic problems with the 100 Hz power supply

system and that the 100 Hz laser system can be delivered in March 81. Application at ASDEX is envisaged for summer 1981.

b) A laser concept for the proposed JET scattering system

As pointed out already in Part 1 of the design study the laser should emit at least 1 Joule of energy to ensure reasonable signal to noise ratios for single spatial point measurements. This value has to be increased by a factor of about 5 when multi spatial point measurement is envisaged. Such an energy can be obtained either by using a single oscillator-amplifier chain or by operating several lasers in parallel. This latter possibility becomes attractive when oscillators are available which emit sufficient energy to saturate already the first subsequent amplifier. Then the volume of the active medium needed to generate a certain energy is the same for a single oscillator-amplifier chain as for several lasers operated in parallel. The operation in parallel will now be considered in more detail since it offers some advantages compared with the more conventional approach.

Of course the most difficult problem arising from parallel operation is how to combine the beams into a single one suited for a scattering experiment. This obviously requires beams of low divergence. In the following we will discuss the possibilities offered by already existing laser systems. A number of producers (e.g. Quantel, Molectron) offer serial systems which emit 0.7 J at 20 Hz repetition rate. The beam diameter is 7 - 8 mm and the beam divergence is 0.6 - 1.5 mrad (full angle).

Ten of these laser beams can be combined by mirrors to form an array of parallel beams shown in cross section in fig. 1. Synchronising the lasers with an accuracy better than the gating time of the detection system is easily feasible. Fig. 2 points out that a number of different combinations of timing the lasers is possible:
High pulse energy operation (7 J) at 20 Hz repetition rate (fig. 2 a). By synchronising the lasers in groups higher repetition rates at lower pulse energies (40 Hz, 3.5 J; 60 Hz, 2.1 J; 100 Hz, 1.4 J) can be achieved (fig. 2b - d).
Furthermore the laser system can emit periodically bursts of pulses. Within such a burst

measurements can be performed at a repetition rate limited only by the speed of the data acquisition.

The described array of laser beams can be focused in different ways. For a single point measurement with high accuracy one would expand the beam by a large factor and focus it to a short, small diameter beam waist. Measuring the profile along the whole plasma diameter calls for no beam expansion (e.g. using Molectron MY 34-20 lasers) which together with a focal length of 6 m yields a beam waist of less than 16 mm diameter over the whole plasma diameter.

The concept of passing the laser beam twice through the plasma by means of a retro-reflector as reported in part 1 of the design study is maintained.

It should be noted that the proposed laser set-up using lasers operated in parallel besides offering high flexibility of operation is relatively insensitive against failures: The break-down of one laser causes only a slight reduction in energy (by 10 %). On the other hand a failure in the oscillator of a single oscillator-amplifier chain inhibits entirely the diagnostics. An amplifier stage which is not operated reduces the output typically by a factor of 2 to 3 and thus also prevents any reliable measurements.

With regard to a possible laser development for the quasicontinuous scattering experiment the use of oscillators only (operated in parallel) would be very promising. Required is an output energy of approx. 1 J, a beam divergence of not more than 1 mrad and a repetition rate of at least 20 Hz. Oscillators which emit 200 mJ at 20 Hz repetition rate with a beam divergence of less than 1 mrad are state-of-the-art /1-4/. According to JK Lasers an increase in both energy and repetition rate seems realistic.

The use of oscillators only would solve the problem of isolating the lasers against optical feedback from the retroreflector. When laser systems with amplifiers are used Faraday rotators or an electrooptical shutter must be applied for optical isolation.

2) Detection optics for obtaining spatial profiles

The detection optics described in the following will afford windows as indicated in fig. 3. The windows will be made of quartz with diameters of

60 mm for laser input
150 mm for laser output and
250 mm for the two observation windows.

The optical path of the laser beam is the same as described in part 1 of the design study. It traverses twice the torus vessel and is then dumped near the laser system.

There are 2 problems connected with the collection optics:

1) imaging of the long scattering volume and its division in a number of individual channels

2) transfer of scattered light out of the torus hall to the detection system.

Since the observed cross section of each scattering volume has a dimension of less than 2 cm and will be observed with f-numbers of 12 - 22 an overall image reduction of up to 6 is necessary to get all the scattered light onto the 3 mm-diameter-detectors. The corresponding f-number on the image side of the optics will therefore be up to f/2.5. Since it is intended to use fibre optics for the transmission of the scattered light it is reasonable to reduce the image size by the given amount already with the collection optics.

Imaging of the scattering volume can be performed either by pure reflective or pure refractive optics or by a combination of both. However, f/2.5-reflective optics will introduce large losses. We therefore envisage a refractive optics, which according to Fa. Zeiss will not be a problem. To avoid radiation damage the path of rays is bent and the f/2.5-optics is located in a shielding tower.

Collecting and focusing optics are coupled rigidly as described in part 1 of the design study. This measure ensures insensitivity against vibrations.

Spatial Point no.	Torus Radius R/mm	Spatial Resolution R/mm	Scattering Angle /deg	Solid Angle d /sr	f# obj	f# imag	Image Size Height x Width mm^2
1	1813	5	3.9	1.6×10^{-3}	22.1	3.5	3.3x2.9
2	1839	44	4.1	1.8	20.9	3.5	3.4x2.4
3	1903	79	4.4	2.0	19.8	3.5	3.6x2.2
4	1997	104	4.6	2.3	18.8	3.5	3.7x2.0
5	2113	121	4.9	2.5	17.8	3.5	3.9x1.8
6	2243	131	5.1	2.8	16.8	3.4	4.1x1.6
7	2381	137	5.4	3.0	15.9	3.4	4.3x1.3
8	2523	139	5.7	3.4	15.1	3.4	4.5x1.2
9	2666	140	6.0	3.8	14.3	3.4	4.7x1.0
10	2808	138	6.4	4.3	13.5	3.3	4.9x1.4
11	2949	135	6.7	4.8	12.8	3.3	5.2x1.8
12	3079	121	4.8	3.7	14.6	2.6	2.3x1.5
13	3202	117	4.9	3.8	14.3	2.6	2.3x1.6
14	3319	114	5.0	4.0	14.0	2.6	2.2x1.8
15	3434	110	5.1	4.2	13.7	2.7	2.2x2.0
16	3544	106	5.2	4.4	13.4	2.7	2.3x2.2
17	3651	101	5.3	4.6	13.1	2.7	2.3x2.3
18	3753	97	5.4	4.7	12.9	2.7	2.2x2.5
19	3850	94	5.5	4.9	12.6	2.7	2.2x2.7
20	3944	90	5.6	5.1	12.4	2.7	2.2x2.9
21	4034	86	5.7	5.3	12.2	2.7	2.2x3.2
22	4120	82	5.8	5.5	12.0	2.7	2.2x3.7

Table 1

Spatial Point no.	Torus Radius R/mm	Spatial Resolution R/mm	Scattering Angle /deg	Solid Angle d /sr	f# obj	f# imag	Image Size Height x Width mm^2
1	1813	5	3.9	1.6×10^{-3}	22.1	3.5	3.3x2.9
2	1839	44	4.1	1.8	20.9	3.5	3.4x2.4
3	1903	79	4.4	2.0	19.8	3.5	3.6x2.2
4	1997	104	4.6	2.3	18.8	3.5	3.7x2.0
5	2113	121	4.9	2.5	17.8	3.5	3.9x1.8
6	2243	131	5.1	2.8	16.8	3.4	4.1x1.6
7	2381	137	5.4	3.0	15.9	3.4	4.3x1.3
8	2523	139	5.7	3.4	15.1	3.4	4.5x1.2
9	2666	140	6.0	3.8	14.3	3.4	4.7x1.0
10	2808	138	6.4	4.3	13.5	3.3	4.9x1.4
11	2949	135	6.7	4.8	12.8	3.3	5.2x1.8
12	3079	121	4.8	3.7	14.6	2.6	2.3x1.5
13	3202	117	4.9	3.8	14.3	2.6	2.3x1.6
14	3319	114	5.0	4.0	14.0	2.6	2.2x1.8
15	3434	110	5.1	4.2	13.7	2.7	2.2x2.0
16	3544	106	5.2	4.4	13.4	2.7	2.3x2.2
17	3651	101	5.3	4.6	13.1	2.7	2.3x2.3
18	3753	97	5.4	4.7	12.9	2.7	2.2x2.5
19	3850	94	5.5	4.9	12.6	2.7	2.2x2.7
20	3944	90	5.6	5.1	12.4	2.7	2.2x2.9
21	4034	86	5.7	5.3	12.2	2.7	2.2x3.2
22	4120	82	5.8	5.5	12.0	2.7	2.2x3.7

Table 1

In order to reduce the requirements on the collection optics two systems are proposed (figs. 3 and 4). The systems image the inner and outer part of the plasma diameter respectively. Considering the optics for the inner part of the plasma diameter the maximum solid angle of the collection system (f/12) is determined by the size of the largest available quartz window (250 mm dia.) and its distance from the nearest scattering volume in the plasma (located at the plasma centre). Then chosing a f = 1000 mm lens, this lens should have a diameter of 450 mm to image the whole inner part of the scattering volume without vignetting.

In case of the second collection optics which image the outer part of the laser beam an unreasonable large lens size would result using the whole aperture of the 250 mm dia. observation window. Therefore the same type of lens is chosen as used for the other collection system. Contrary to the collection optics for the inner part, the solid angle of observation for the second system is then determined by the size of the imaging lens (fig. 4).

By positioning quartz lenses of long focal length ($f \approx 4.3$ m, f/16 and $f \approx 2.5$ m, f/10) near the observation windows, the size of the high quality, large f-number lenses positioned in the shielding tower can be reduced.

The transmission of the collection optics including the window is assumed to be 0.6.

With both optical systems the image of the extended scattering volume is a straight line inclined versus the optical axis according to the "Scheimpflug"-condition (see fig. 5). The images can be divided into a number of individual channels defining the spatial resolution by means of fibre optics (or small mirrors) as indicated in fig. 5. There is a small amount of cross-talk near the edges of adjacent channels due to the finite solid angles. This vignetting, however, occurs only for one direction of the incident rays. Therefore the reduction of spatial resolution remains small.

There exist two possibilities for transmitting the collected light to the detection system located outside the torus hall:

1) fibre optics which are already used for defining the individual scattering volumes.
2) a relaying system of lenses as used in periscopes.

Of course, handling of the fibre optics is more comfortable than to set up the periscopes. Therefore fibre optics would be preferred if they are suited for this purpose due to their physical parameters.

The only known type of fibre fitting to the requirements is the high purity fused quartz fibre (Fiberguide Industries) proposed for use on TFTR and also by JET design study 8.2. Its main physical parameters are (see data sheet no 1):

1) Core-fibre area ratio of 80 % which leads to a theoretical geometrical bundle efficiency of 72 %. The producer specifies a value of > 60 % for manufactured bundles (up to f/2).
2) Transmission at 1 μm (see JET design study 8.2) is less than 10 dB/km. This yields losses of less than 10 % for a necessary length of about 50 m.

Thus the overall transmission of the collection and transmission optics including the fibre optics is about 25 %.

The use of these fibre optics would also allow to change the rectangular image cross section to a circular one which is adapted to the active area of serial commercially available detectors.

Of couse the proposed system using fibre optics critically depends on the availability of this special type of fibres (only one producer known at the present), on their actual transmission losses and on their radiation resistance. Therefore tests are urgently required.

Short fibre optics (transmission $\approx$ 50 %) would also present a simple means to dissect the extended image of the whole scattering volume into individual spatial channels if the second possible solution is chosen. In this case the ends of the fibre bundles could then be rearranged within a circular area. This measure would facilitate the application of a single periscope with large cross section. Another possibility is the use of a number of

periscopes. Then the requirement on the periscope optics could be reduced.

At input and output of the relaying periscope system a high f-number lens ($\sim$ f/2.5, transmission $\sim$ 0.8) is needed. The relay system itself consists of about 20 lenses of small aperture ($\sim$ f/15, transmission $\sim$ 0.98) for covering the approximate 40 m distance.

The overall transmission of collection and transmission optics up to the spectrometer is 12 % for this solution.

3) Spectrometers

The spectrometers must be capable of resolving the smallest spectral bandwidth considered for an individual spatial point ($\Delta\lambda_{min} \approx$ 2.0 nm for the spatial point no. 2) and must show highest possible transmission for both components of polarization (the scattered light is unpolarized). Furthermore its étendue must be at least 1.5×10^{-2} $cm^2 sr$. These requirements can be met by a filter polychromator arrangement described by Mahdavi /7/.

The Mahdavi set-up shown in fig. 6 is used to measure unpolarized scattered light. Assumed is a value of 98 % for transmission and reflection efficiency of the polarizing cube (CVI specification: T = 98 %, R = 99.5 %), a transmission of the quarter wave retardation plates of 98 % and a reflection and transmission efficiency of the interference filters of 70 %. Thus an overall transmission of the spectrometer for unpolarized light of 50 % results.

This value is further decreased by a factor of about 0.7 since an additional interference filter will be used in each spectral channel for stray light suppression.

The parameters of the proposal extended to spatial scan are summarized in table 2:

Table 2

	inner plasma radius	outer plasma radius
No. of spatial points	11	11
spatial resolution	R = 0.5 - 14 cm	R = 8 - 12 cm
scattering angle	4° - 7°	5° - 6°
solid angle of observation	$1.6 - 4.8 \times 10^{-3}$ sr	$3.7 - 5.5 \times 10^{-3}$ sr
transmission of collection and detection optics	5 % - 9 %	

4) Recent improvements in detector technology

RCA in the meantime has achieved a major improvement in the quantum efficiency of their Si avalanche photodiodes. The quantum efficiency at 1.06 μm is now 45 % and thus superior to that of the General Electric avalanche photodiodes. The RCA diodes can be delivered with customer specified sensitive area cross sections (e.g. rectangular) and with integrated preamplifiers. The specifications for a 7 mm^2 area Si avalanche photodiode including an integrated preamplifier are:

gain M	= 60
quantum efficiency	= 45 % at 1.06 μm
excess noise factor F	= 3 at full gain
NEP	= 1.6×10^{-13} W $Hz^{-1/2}$ at 20 MHz bandwidth

Diodes of 7 x 1 mm^2 sensitive area of this type have recently been delivered by RCA for the scattering experiment on ASDEX (see data sheet no. 2).

5) Minimum errors attainable by the two channel ratio method

Due to the change to a spatial multi-channel detection system the use of two channel spectrometers becomes attractive. This method is discussed in detail e.g. by /5,6/. It offers in our case - besides reducing the number of detectors - the advantage that the effect of the detector noise on the SNR is reduced (the width of the spectral channels is larger than in the case of a multichannel detection system and therefore more photons impinge on each detector). We therefore propose to use this technique for the quasi-stationary scattering system.

In the following the minimum attainable errors due to the statistics are estimated for the case that the two channel ratio method is used.

For the determination of the signal to noise ratio for each channel the detector specifications and the parameters of the detection optics as given above are used. The enhancement factor of the plasma background radiation is taken to be 100 and the gating time of the electronics is chosen to be 50 ns.

As has been shown in part 1 of the design study the deviations of the scattered spectrum from a Gaussian distribution are small within a wide range of temperatures. We have therefore used the nonrelativistic spectra for the calculation of the errors of the electron temperature. This procedure simplifies the evaluation of the numbers of scattered photons within each spectral channel since the tabulated error function can be used.

The blue wing of the spectrum is observed with two spectral channels according to fig. 7. For this situation the fractions of the total number of scattered photons within each channel are listed in table 3. The ratio R of the photon numbers within the two spectral channels as function of the electron temperature is determined and depicted in fig. 8.

For 6 representative spatial points the signal to noise ratios for each spectral channel were calculated according to the formulae given in part 1, p. 29, Nr. (22, 23). These errors in the measurements are then proceeded to yield the error of the signal ratio R according to

$$\frac{\Delta R}{R} = \left[\left(\frac{S}{N}\right)_1^{-2} + \left(\frac{S}{N}\right)_2^{-2} \right]^{1/2}$$

The error of the electron temperature is determined graphically from fig. 8. Figs. 9 and 10 show the errors in electron temperature for different temperatures at electron densities of 1×10^{13} cm^{-3} and 1×10^{14} cm^{-3} respectively. For these calculations all spectrometers were optimized for Te $\approx$ 1 keV (equal numbers of scattered photons in both spectral channels). The given errors correspond to a laser energy of 3.5 J in the scattering volume. Assuming a transmission of the laser optics of 0.5 this is achieved in the described 20 Hz operation mode.

$\frac{\Delta\lambda_{channel}}{\Delta\lambda_{1/2}\,(1\ keV)}$ / T_e / keV	0 - 0.25	0.25-0.75	0.75-2.5	Σ
0.5	16.74 %	23.55	9.71	50.00
0.75	13.81	21.73	14.44	49.98
1.	12.02	20.05	17.82	49.89
2.	8.57	15.62	24.29	48.47
3.	7.01	13.18	25.95	46.14
4.	6.08	11.61	26.01	43.7
5.	5.44	10.5	25.5	41.4

Table 3

6) New calibration techniques

As already proposed at the last workshop on Thomson scattering at the JET torus, Raman scattering should be used for density calibration of Thomson scattering systems. The advantage of Raman scattering as compared with Rayleigh scattering for this purpose is the frequency shift of Raman scattered light. This shift offers the possibility for calibration even in such cases in which the unshifted Rayleigh scattering signal is not detectable due to high straylight level. Furthermore the Raman scattering signal is not disturbed by Mie scattering of microscopic dust particles. The latter is of special importance in forward scattering systems and may cause an overestimate of Rayleigh scattering calibration signal. At the last workshop we proposed the use of SF_6 as a Raman scattering medium using its fundamental vibrational Stokes line. SF_6, however, seems to be an unproper gas in tokamaks because it may stick at dipole molecules like H_2O at the wall due to its high polarizability. In the following discharges it may cause too high an impurity level in the plasma.

For this reason we looked for the rotational Raman cross sections of hydrogen and deuterium-following the proposal of /8/ - two gases which should be allowed in a fusion experiment.

The frequency shift of both molecules is large enough for application in a scattering experiment at JET because of the small momentum of inertia of H_2 and D_2.

Therefore we measured and calculated the ratio of Raman to Rayleigh cross-section for hydrogen and deuterium. The measurement was done in a scattering cell near atmospheric pressure using an argon ion laser and lock-in technique. In this experiment we could determine the cross sections of the first three rotational Stokes lines. The statistical error for the most intense lines is of the order of 10 % for the ratio Raman/Rayleigh cross section.

Because of the simplicity of the hydrogen/deuterium molecules we also could calculate

the ratio Raman/Rayleigh cross section using data for polarizability and its anisotropy from literature /9, 10/.

Calculated and measured values agree within the error bars. In table 4 and 5 calculated values of Stokes and Antistokes lines of hydrogen and deuterium are listed. They contain also the electron density which scatters the same as 100 Torr of H_2 and D_2, respectively. The two columns labelled $\parallel \bar{E}_1$ and $\parallel + \perp \bar{E}_1$ take into account the fact that pure rotational Raman scattering has essentially quadrupole characteristics as compared with the Rayleigh and Thomson scattering, which is essentially dipole radiation. So it does make a difference whether one uses a polarization filter in the observation path ($\parallel \bar{E}_1$) or not ($\parallel + \perp \bar{E}_1$).

The relatively large values of the Antistokes lines, especially those of D_2, offer the possibility not only to calibrate ruby laser systems but also the qusistationary Nd-YAG experiment, the detectors of which become insensitive on the red shifted wing of the scattering spectrum. Furthermore, in the quasistationary experiment one has the possibility of integrating over the entire pulse train during calibration so that even small Raman cross sections (Antistokes) prove to be useful for calibration.

A first application has been performed at ASDEX. Using up to 25 Torr H_2 the standard ruby scattering experiment has been calibrated. Stokes as well as Antistokes scattering could be observed.

the ratio Raman/Rayleigh cross section using data for polarizability and its anisotropy from literature /9, 10/.

Calculated and measured values agree within the error bars. In table 4 and 5 calculated values of Stokes and Antistokes lines of hydrogen and deuterium are listed. They contain also the electron density which scatters the same as 100 Torr of H_2 and D_2, respectively. The two columns labelled $\parallel \bar{E}_1$ and $\parallel + \perp \bar{E}_1$ take into account the fact that pure rotational Raman scattering has essentially quadrupole characteristics as compared with the Rayleigh and Thomson scattering, which is essentially dipole radiation. So it does make a difference whether one uses a polarization filter in the observation path ($\parallel \bar{E}_1$) or not ($\parallel + \perp \bar{E}_1$).

The relatively large values of the Antistokes lines, especially those of D_2, offer the possibility not only to calibrate ruby laser systems but also the qusistationary Nd-YAG experiment, the detectors of which become insensitive on the red shifted wing of the scattering spectrum. Furthermore, in the quasistationary experiment one has the possibility of integrating over the entire pulse train during calibration so that even small Raman cross sections (Antistokes) prove to be useful for calibration.

A first application has been performed at ASDEX. Using up to 25 Torr H_2 the standard ruby scattering experiment has been calibrated. Stokes as well as Antistokes scattering could be observed.

Table 4

Calculated Raman Cross Sections for Hydrogen (H_2) [T = 20° C]

Transition	λ = 6943 Å		$\parallel \bar{E}_1$	λ = 6943 Å		$\parallel + \perp \bar{E}_1$	λ = 10590 Å		$\parallel \bar{E}_1$	λ = 10590 Å		$\parallel + \perp \bar{E}_1$
$l \to l'$ / $\Delta\nu$ (cm^{-1})	λ'	$\frac{\sigma_{Raman}}{\sigma_{Rayleigh}}$	100 Torr $\hat{=} \times 10^{12} \frac{e}{cm^3}$	λ'	$\frac{\sigma_{Raman}}{\sigma_{Rayleigh}}$	100 Torr $\hat{=} \times 10^{12} \frac{e}{cm^3}$	λ'	$\frac{\sigma_{Raman}}{\sigma_{Rayleigh}}$	100 Torr $\hat{=} \times 10^{12} \frac{e}{cm^3}$	λ'	$\frac{\sigma_{Raman}}{\sigma_{Rayleigh}}$	100 Torr $\hat{=} \times 10^{12} \frac{e}{cm^3}$
0 → 2 / -354	7118	$\frac{1}{675}$	2,8	7118	$\frac{1}{385}$	4,9	11002	$\frac{1}{720}$	0,52	11002	$\frac{1}{411}$	0,91
1 → 3 / -587	7238	$\frac{1}{240}$	7,8	7238	$\frac{1}{137}$	13,7	11292	$\frac{1}{265}$	1,4	11292	$\frac{1}{151}$	2,45
2 → 4 / -813	7359	$\frac{1}{1733}$	1,1	7359	$\frac{1}{990}$	1,96	11588	$\frac{1}{1990}$	0,19	11588	$\frac{1}{1137}$	0,33
2 → 0 / +354	6776	$\frac{1}{3203}$	0,6	6776	$\frac{1}{1830}$	1,05	10207	$\frac{1}{3078}$	0,12	10207	$\frac{1}{1759}$	0,21
3 → 5 / -1033	7480	$\frac{1}{2750}$	0,68	7480	$\frac{1}{1571}$	1,19	11891	$\frac{1}{3283}$	0,11	11891	$\frac{1}{1876}$	0,20
3 → 1 / +587	6671	$\frac{1}{3223}$	0,6	6671	$\frac{1}{1841}$	1,05	9970	$\frac{1}{3000}$	0,12	9970	$\frac{1}{1714}$	0,22
4 → 6 / -1254	7605	$\frac{1}{74783}$	0,025	7605	$\frac{1}{42733}$	0,044	12212	$\frac{1}{93528}$	0,004	12212	$\frac{1}{53444}$	0,007

Table 5

Calculated Raman Cross Sections for Deuterium (D_2) [T = 20°C]

Transition	λ = 6943 Å		‖ $\bar{E}_1$	λ = 6943 Å		‖+⊥ $\bar{E}_1$	λ = 10590 Å		‖ $\bar{E}_1$	λ = 10590 Å		‖+⊥ $\bar{E}_1$
$l \rightarrow l'$ / $\Delta\nu$ (cm^{-1})	λ'	$\frac{\sigma_{Raman}}{\sigma_{Rayleigh}}$	100 Torr $\hat{=}$ $\times 10^{12} \frac{e}{cm^3}$	λ'	$\frac{\sigma_{Raman}}{\sigma_{Rayleigh}}$	100 Torr $\hat{=}$ $\times 10^{12} \frac{e}{cm^3}$	λ'	$\frac{\sigma_{Raman}}{\sigma_{Rayleigh}}$	100 Torr $\hat{=}$ $\times 10^{12} \frac{e}{cm^3}$	λ'	$\frac{\sigma_{Raman}}{\sigma_{Rayleigh}}$	100 Torr $\hat{=}$ $\times 10^{12} \frac{e}{cm^3}$
0 → 2 / -179	7030	$\frac{1}{470}$	4,2	7030	$\frac{1}{269}$	7,3	10795	$\frac{1}{488}$	0,76	10795	$\frac{1}{279}$	1,33
1 → 3 / -298	7090	$\frac{1}{723}$	2,7	7090	$\frac{1}{413}$	4,8	10935	$\frac{1}{765}$	0,48	10935	$\frac{1}{437}$	0,84
2 → 4 / -415	7149	$\frac{1}{470}$	4,2	7149	$\frac{1}{269}$	7,3	11077	$\frac{1}{505}$	0,72	11077	$\frac{1}{289}$	1,26
2 → 0 / +179	6858	$\frac{1}{1023}$	1,9	6858	$\frac{1}{584}$	3,4	10393	$\frac{1}{1005}$	0,36	10393	$\frac{1}{574}$	0,63
3 → 5 / -530	7208	$\frac{1}{1798}$	1,1	7208	$\frac{1}{1027}$	1,9	11220	$\frac{1}{1970}$	0,18	11220	$\frac{1}{1126}$	0,32
3 → 1 / +298	6802	$\frac{1}{2665}$	0,76	6802	$\frac{1}{1523}$	1,33	10266	$\frac{1}{2560}$	0,14	10266	$\frac{1}{1463}$	0,24
4 → 6 / -643	7267	$\frac{1}{2480}$	0,8	7267	$\frac{1}{1417}$	1,4	11364	$\frac{1}{2728}$	0,13	11364	$\frac{1}{1559}$	0,23

7) Results from a pilot experiment on ASDEX

A test experiment on ASDEX has been performed using a Nd:glass laser emitting 13 J with a pulse duration of 20 ns. Fig. 11 shows schematically the experimental set-up. The laser beam is passed vertically through the center of the plasma and is focused in the horizontal plane ($\varnothing \approx 6$ mm). A Brewster angle Schott KG 3 filter glass plate at the exit window serves as a beam dump. No baffles have been introduced up to now into the vessel to reduce the stray light.

The laser beam is viewed at 90° at the center of the plasma. The detection optics image an area of 25 x 4.2 mm^2 onto the entrance slit of a 0.25 m Jarell-Ash monochromator. No viewing dump is installed. The solid angle of observation is 1.4×10^{-2} sr.

The grating monochromator is modified into a two-channel polychromator: Two lens segments positioned in the focal plane of the polychromator image the focusing mirror onto two tapered light guides. The ends of these rods are in close connection with the sensitive areas of two 3 mm $\varnothing$ GE 50 EHS Si avalanche photodiodes. In the first crude set-up of the collection optics the overall transmission was measured to be 1.2 %. The contribution of the different optical components to this low value is as follows:

Part:	Transmission:
window (ordinary sheet glass)	0.57
lenses (collection optics)	0.8
coloured glass edge filter (discriminating against 2. order)	0.47
interference filter for stray light suppression	0.8

The cross talk between the channels of the polychromator and the attenuation of the 1.06 μm light scattered into these was measured to be 1:1000. Radiation at 1.064 μm was further discriminated by a factor of 1000 with the help of a 16-cavity interference filter.

The signals of the photodiodes were fed to commercially available integrated trans-impedance amplifiers (TIEF 152) followed by a further amplifier stage. The sensitivity of the spectral channels was measured with a pulsed light source filtered spectrally by another monochromator. The power of the spectrally filtered (tunable) light source at different wavelengths was calibrated relative to each other with a power meter.

The major problem of the measurements turned out to be the high stray light level caused by the broad spectral emission of the Nd:glass laser. With the help of a Lyot-filter placed in the laser oscillator/11/the stray light level in both channels was reduced to a tolerable magnitude (lower than that of the scattered light).

Fig.12 presents typical recordings with this preliminary arrangement. The oscillograms of two shots, one with plasma and one without, are shown.

The results of the experiments which are relevant to the proposed scattering experiment on JET are summarized in the following:

1) The enhancement factor of the bremsstrahlung radiation at 950 nm was determined from the dc current of the photodiodes and from the values of T_e and n_e derived from independent measurements (ruby scattering, interferometry, ECE). Its value turned out to be of the order of 100 for the investigated set of ASDEX discharges. An exact value cannot be stated yet since the observed plasma volume is not defined precisely (no viewing dump).

2) The noise due to plasma radiation was investigated with a spectrum analyzer in the frequency range up to 50 MHz. A comparison with the noise due to an incandescent lamp creating the same dc current of the photodiodes indicates no deviation from shot noise behaviour.

3) The absolute values of the signals of the scattered light are in close agreement with the calculated ones using the measured parameters of the set-up. They indicate a laser energy of 8 J in the observed plasma volume.

4) The SNR of the scattered light signal was measured to be 16 in spectral channel 1

(close to the laser line) and 11 in channel 2. Using the plasma parameters measured independently and the calibrated sensitivity of the detection system, the corresponding theoretical values are 20 and 15, respectively.

(With regard to fig. 12 it should be noted that most of the noise on the trace stems from rf interference due to the Pockels cell pulser in this preliminary set-up).

5) A direct comparison of the parameters of the proposed scattering experiment on JET with those of the experiment performed on ASDEX is given in the table below:

	ASDEX 90°		JET 8°	
	700 eV, 2×10^{13} cm^{-3}		1 keV, 1×10^{13} cm^{-3}	
	K = 100, T = 0.012		K = 100, T = 0.1	
	$2.5\times0.4\times80$ cm^3		$1.5\times1.5\times800$ cm^3	
	$d\Omega = 1.4\times10^{-2}$ sr		$d\Omega = 8\times10^{-3}$ sr	
	8J		0.7 J	
	channel 1	channel 2	channel 1	channel 2
no. of scattered photons on detector	7×10^3	5×10^3	5.2×10^3	4.6×10^3
no. of plasma radiation photons	3×10^2	1×10^3	3.4×10^3	1.2×10^4
no. of photons equivalent to detector noise (n_D/F)	2×10^3	2×10^3 (GE diode)	2.7×10^3	2.7×10^3 (RCA diode)
	experimental values		predicted values	

Since the experimentally observed SNR values on ASDEX agree well with the predicted ones, the performed scattering experiment represents a relevant test of the detector characteristics on which the proposed experiment on JET is based.

Figure Captions

Fig. 1 Array of parallel laser beams

Fig. 2 Timing of the lasers

Fig. 3 Position of observation windows and distribution of spatial channels

Fig. 4 Imaging optics (schematic)

Fig. 5 Fibre optics array for outer plasma radius

Fig. 6 Proposed spectrometer (Mahdavi)

Fig. 7 Spectral channel distribution for a two channel spectrometer.

Fig. 8 Ratio of number of scattered photons within two spectral channels versus electron temperature.

Fig. 9 Error of electron temperature measurement versus tokamak radius. Spectrometers optimized for 1 keV, $n_e = 1 \times 10^{13}$ cm^{-3}

Fig. 10 Same as Fig. 9, $n_e = 1 \times 10^{14}$ cm^{-3}

Fig. 11 Scattering arrangement on ASDEX

Fig. 12 Typical results from the first measurements on ASDEX
Distribution of spectral channels:
K_{-1}: 987 nm - 1059 nm / K_{-2}: 882 nm - 1014 nm

References

/1/ D. Andreou: "The construction and performance of a 20 pps unstable ND:YAG oscillator", Report CLM-P507 (77)

/2/ R.L. Byer, R.L. Herbst: "The unstable-resonator yag", Laser Focus, July 76, p. 48
"A 200 mJ unstable resonator Nd:YAG oscillator", Optics Comm. 21, 5 (77), Quanta - Ray, data sheet

/3/ D.C. Hanna, L.C. L aycock: "An unstable resonator Nd:YAG laser" Optical and Quantum Electronics 11, 153 (79)

/4/ P.H. Sarkies: "A stable YAG resonator yielding a beam of very low divergence and high output energy", Optics Comm. 31, 189 (79)

/5/ M.J. Forrest, P.A. Jones, N.J. Peacock, R. Prentice, A.C. Selden, C.I. Walker, S. Ward: "JET design study 8.2, Spatial scan Thomson scattering"

/6/ J. Lasalle, P. Platz, Opt. Comm. 17, 325 (76) and
Report EUR-CEA-FC-987, Fontenay-aux-Roses (79)

/7/ M.A. Mahdavi: "Compact interference-filter polychromator and narrow band rejection filter", Applied Optics 7, 1765 (77)

/8/ J. Howard, B.W. James, W.B. Smith, J. Phys. D 12, 1435 (79)

/9/ A.L. Ford, J.C. Browne, Phys. Rev. A 7, 418 (73)

/10/ N.J. Bridge, A.D. Buckingham, Proc. Roy. Soc. London z95, 334 (66)

/11/ Y.S. Liu: "Line narrowing and tuning of a high-power Nd:glass laser using an intracavity Brewster-angle birefringent filter", J. Appl. Phys. 48, 647 (77)

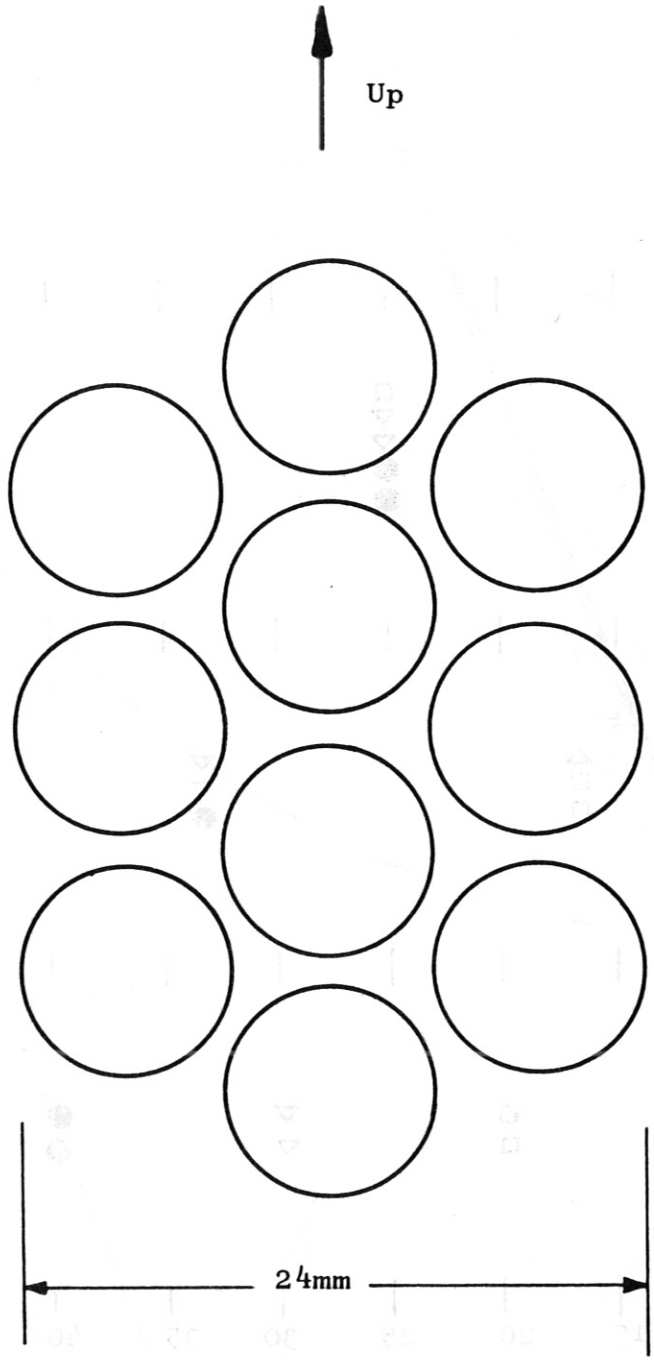

Fig. 1

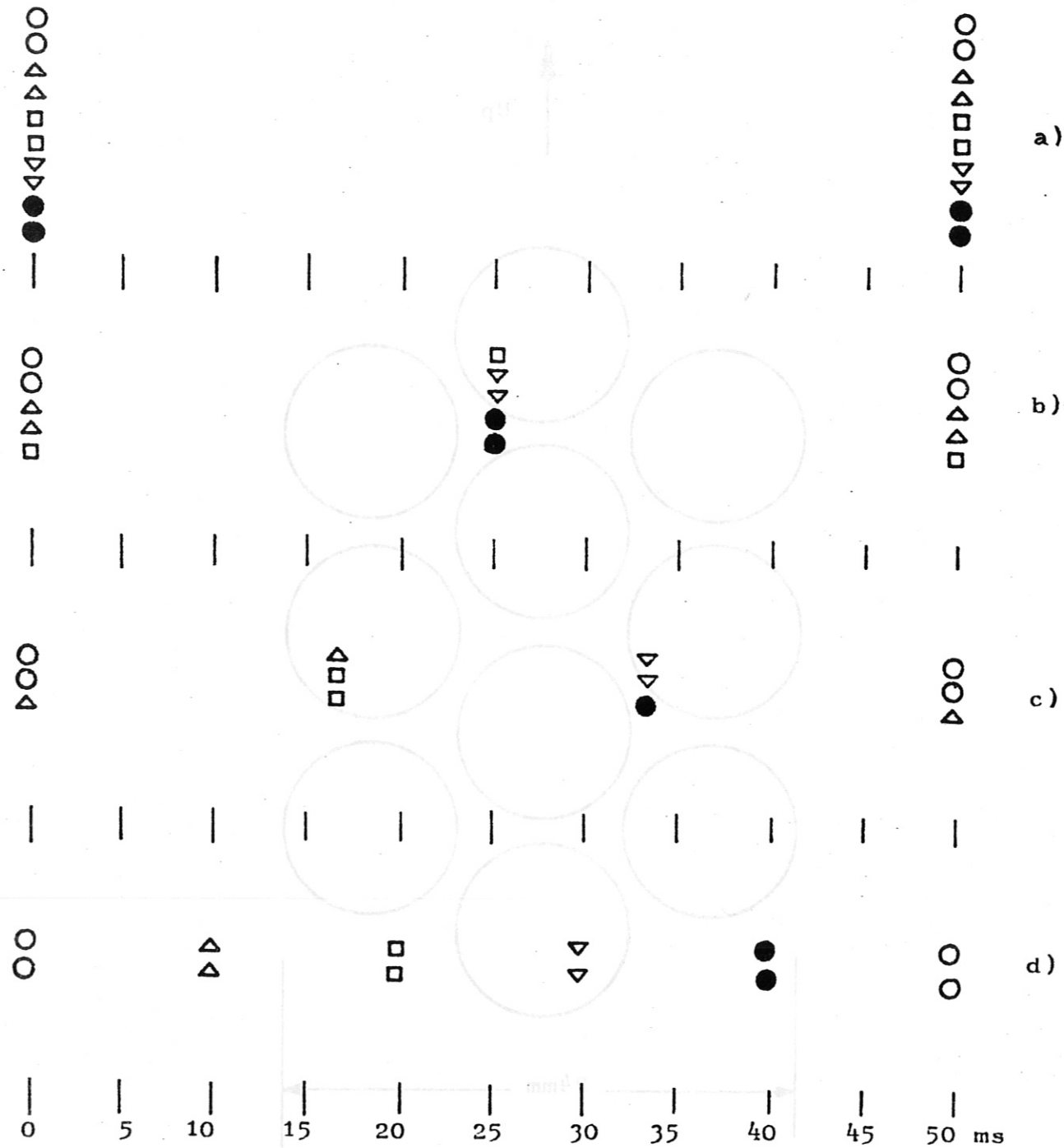

Fig. 2

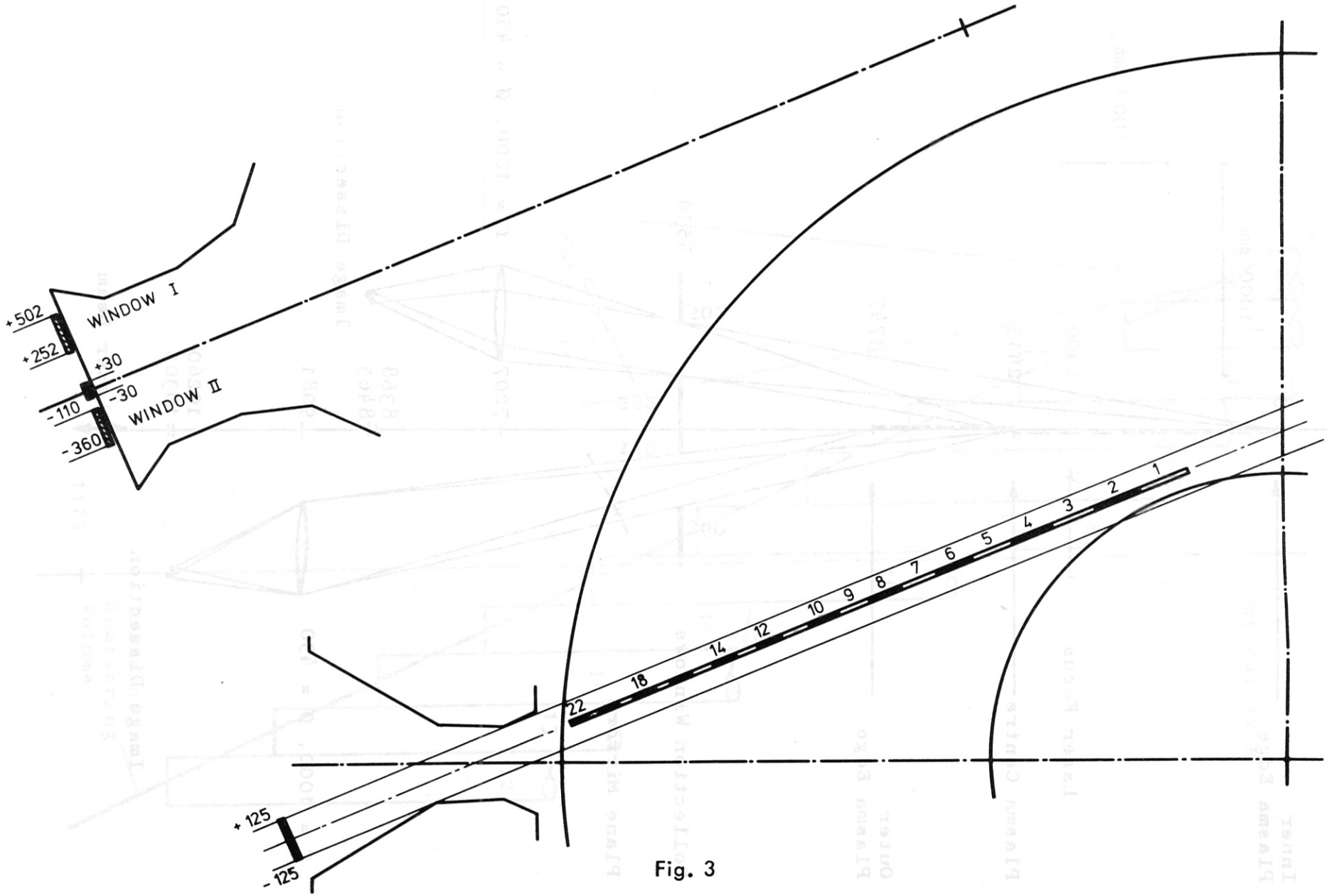
+502
+252
WINDOW I
+30
-30
-110
WINDOW II
-360
+125
-125
1
2
3
4
5
6
7
8
9
10
12
14
18
22

Fig. 3

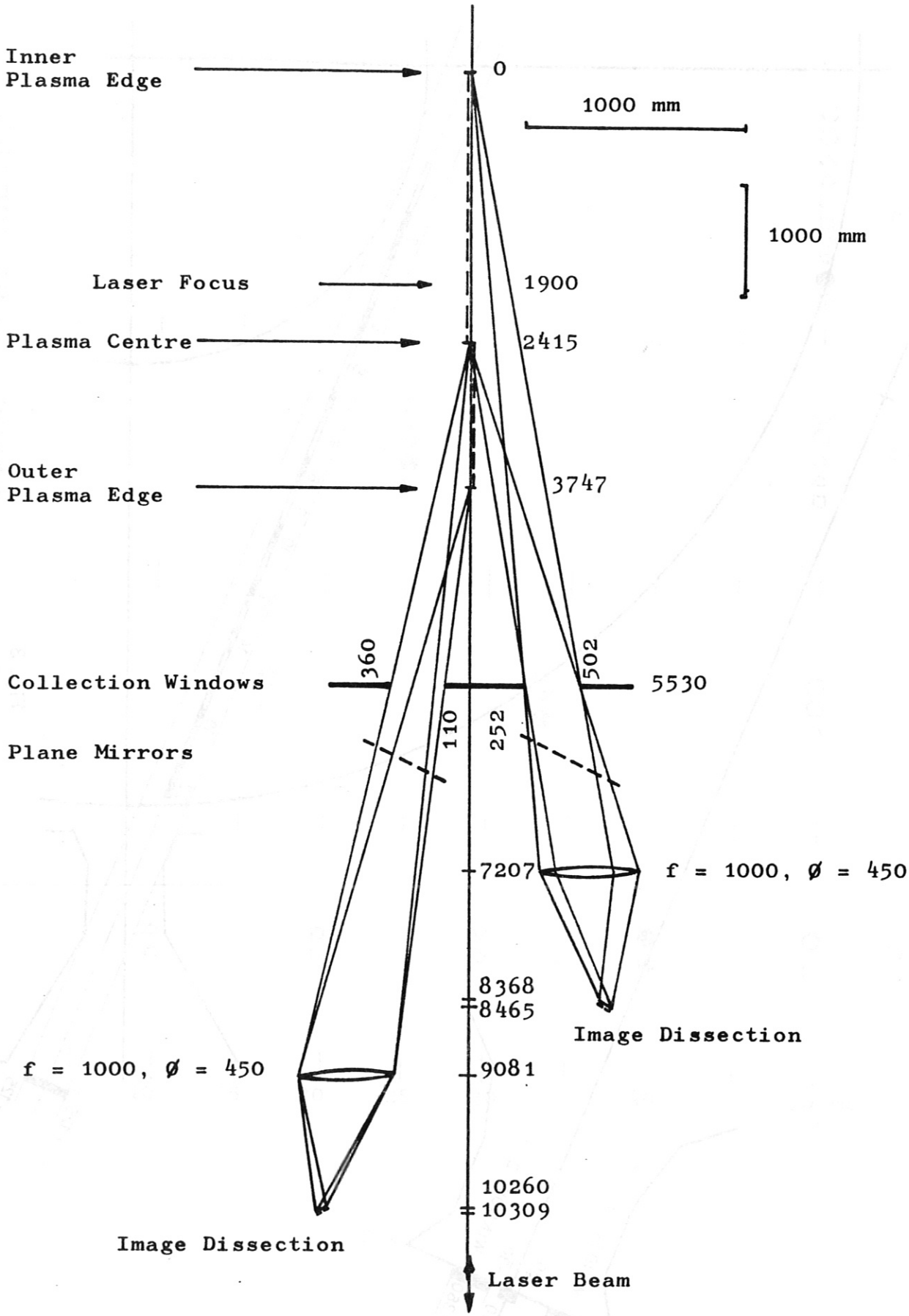
Inner
Plasma Edge
0
1000 mm
1000 mm
Laser Focus
1900
Plasma Centre
2415
Outer
Plasma Edge
3747
360
502
Collection Windows
5530
110
252
Plane Mirrors
7207
f = 1000, Ø = 450
8368
8465
Image Dissection
f = 1000, Ø = 450
9081
10260
10309
Image Dissection
Laser Beam

Fig. 4

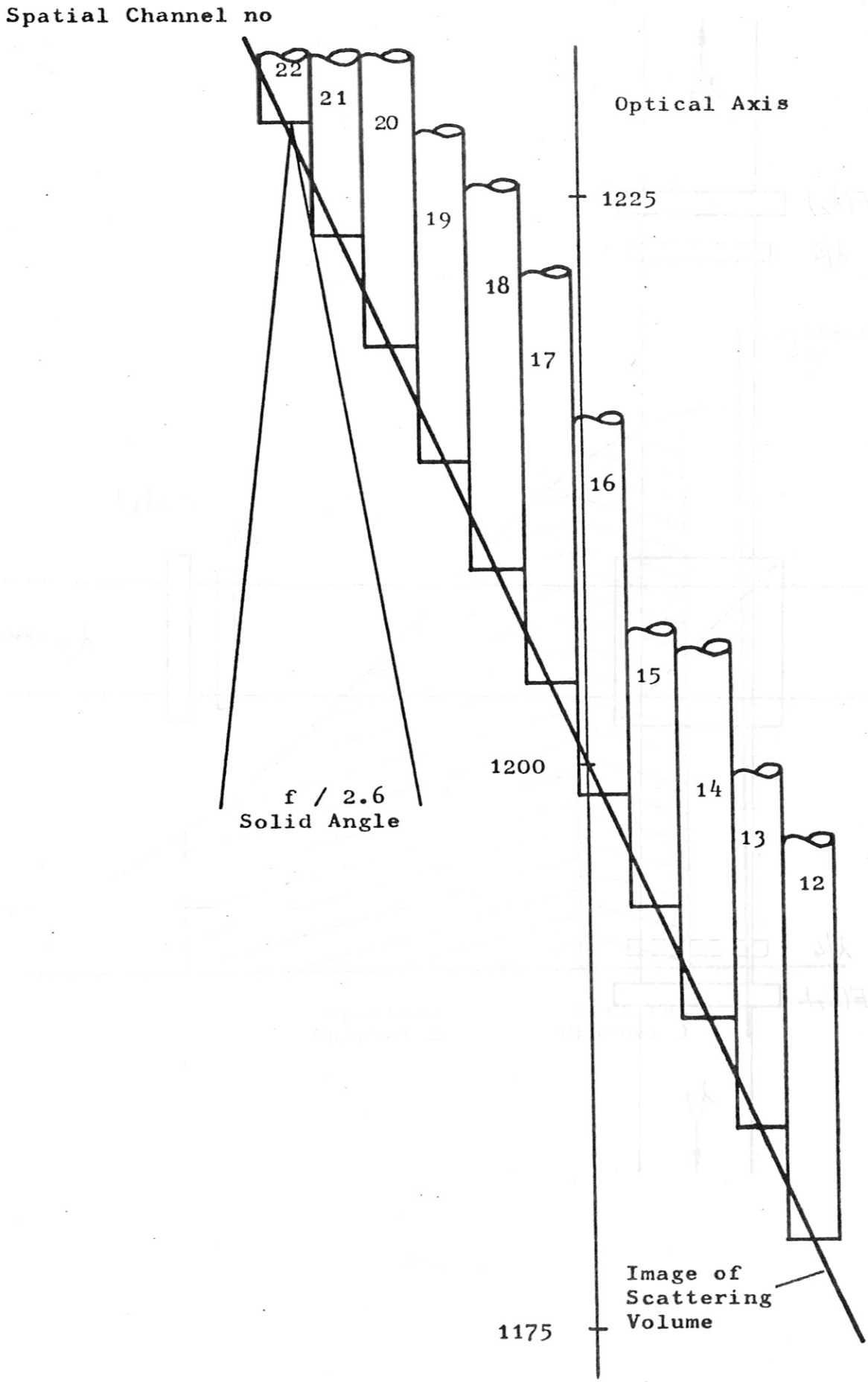
Spatial Channel no
22
21
20
19
18
17
16
15
14
13
12
Optical Axis
1225
1200
1175
f / 2.6
Solid Angle
Image of
Scattering
Volume

Fig. 5

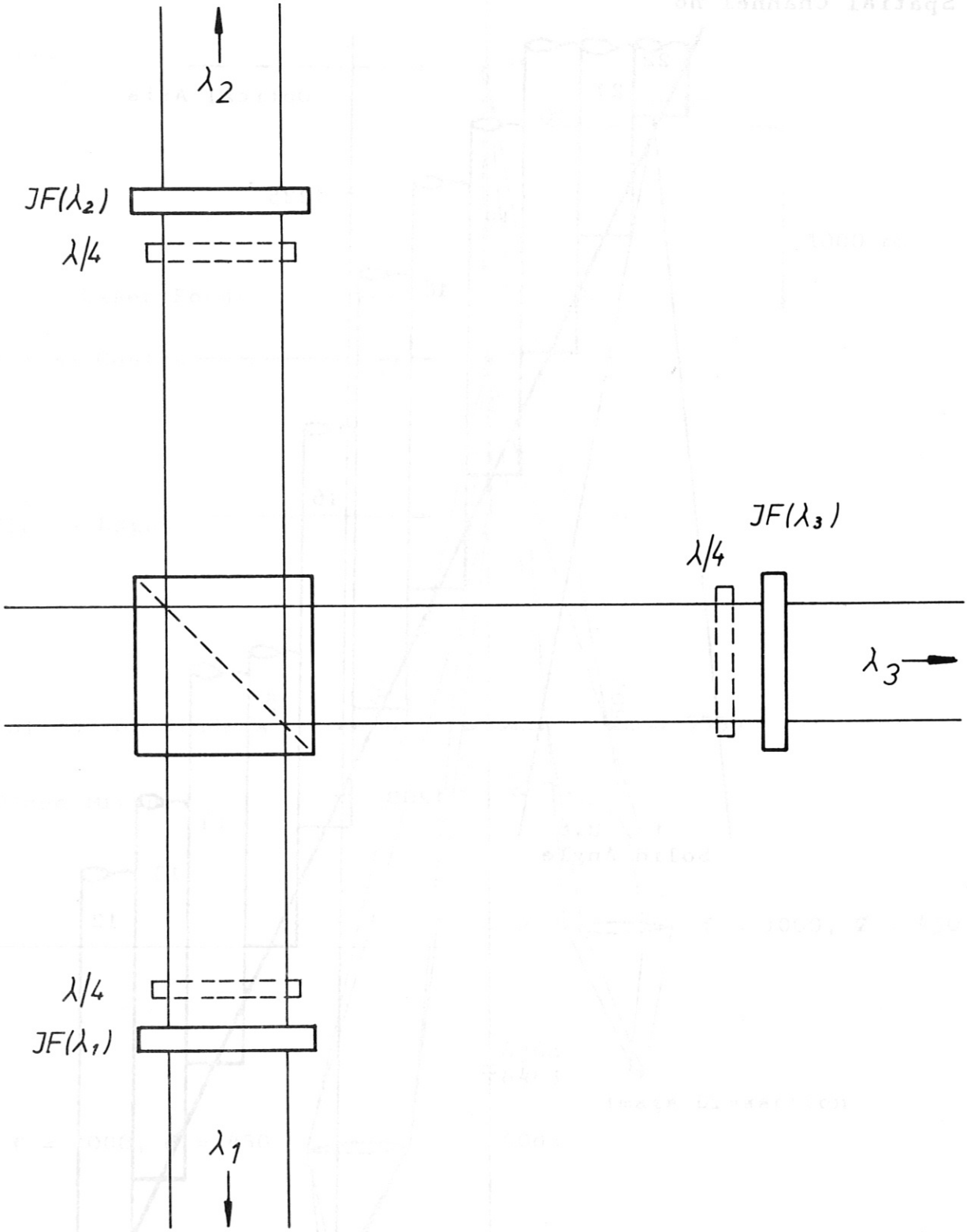

Fig.6

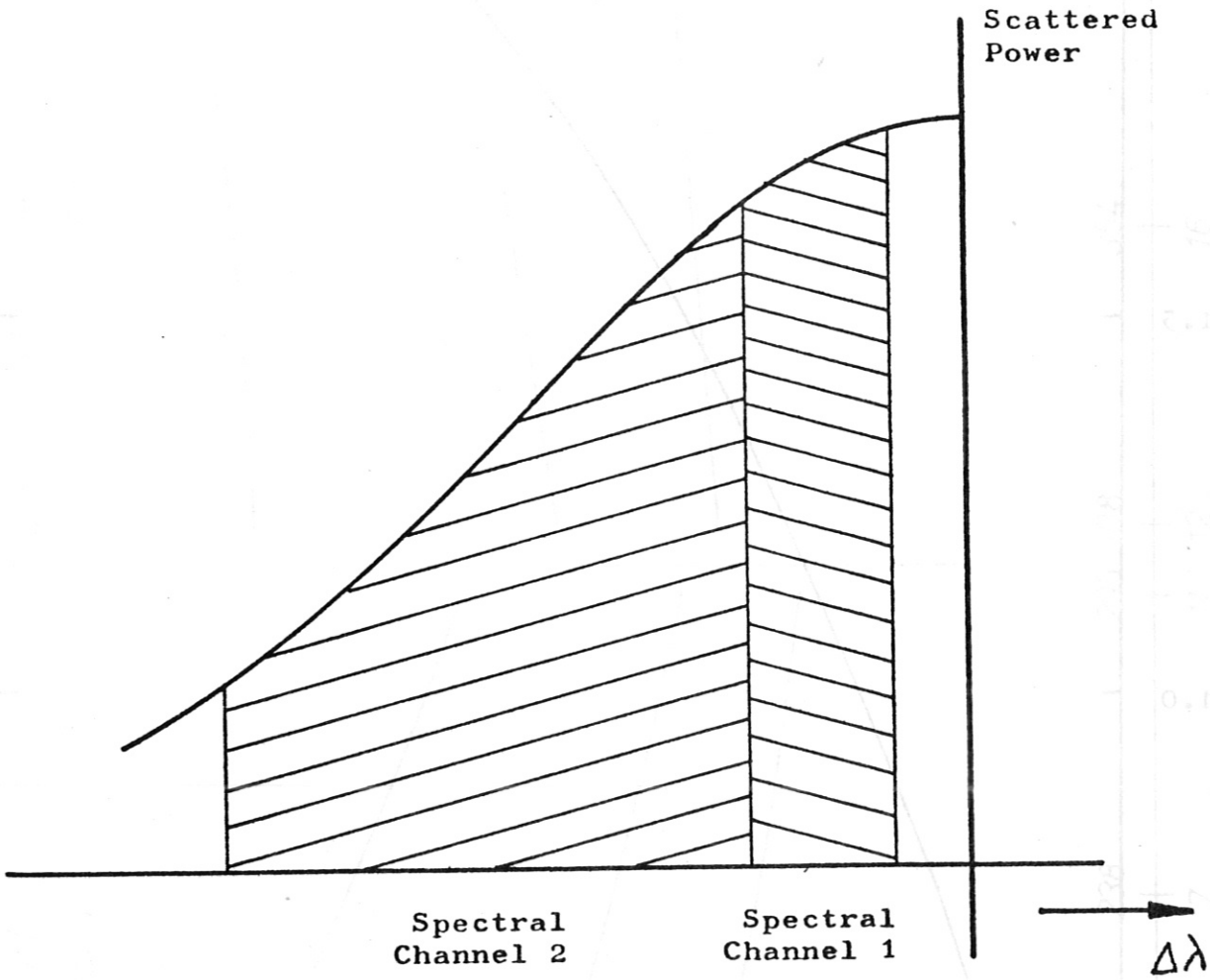

Fig. 7

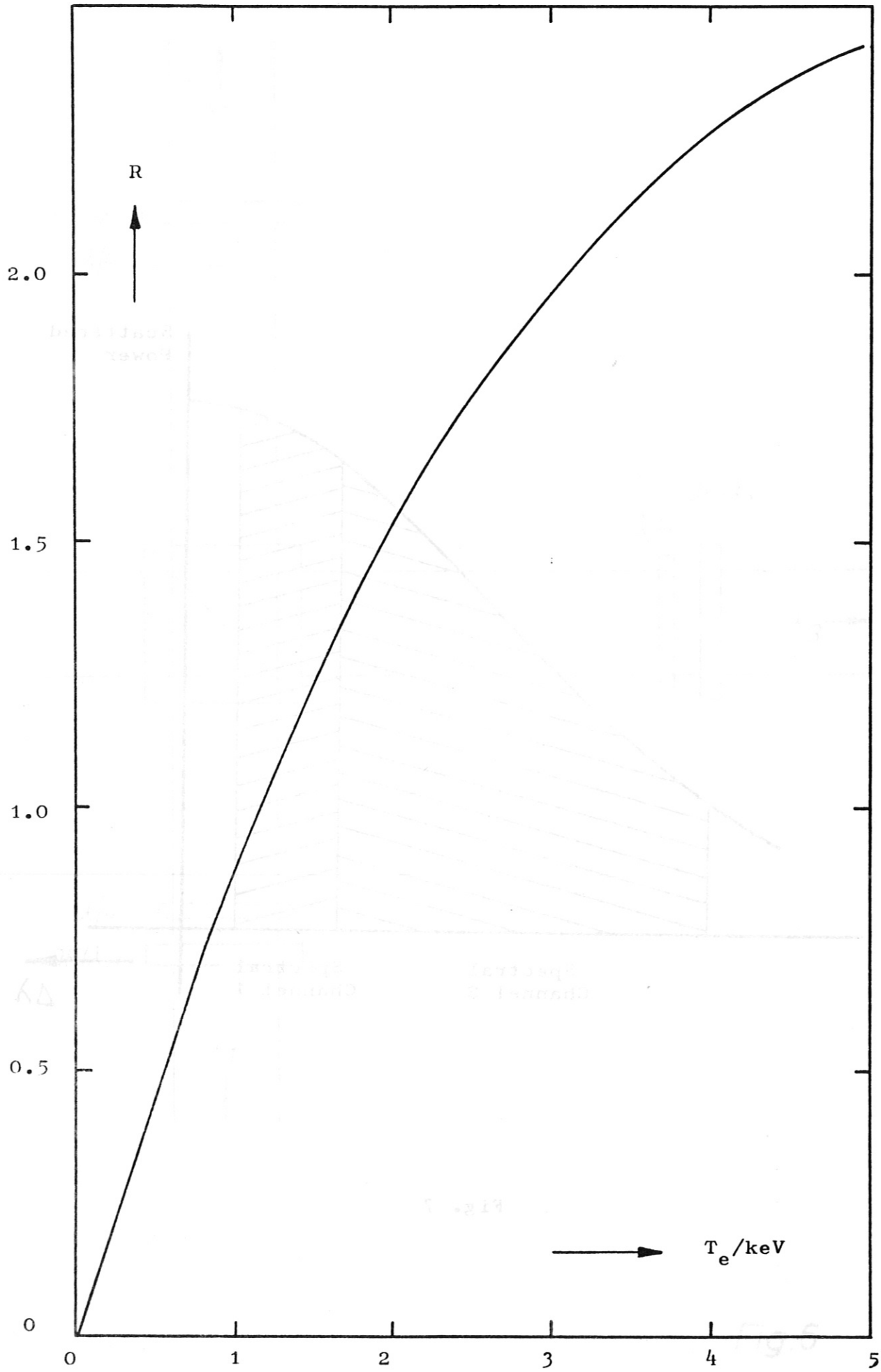

Fig. 8

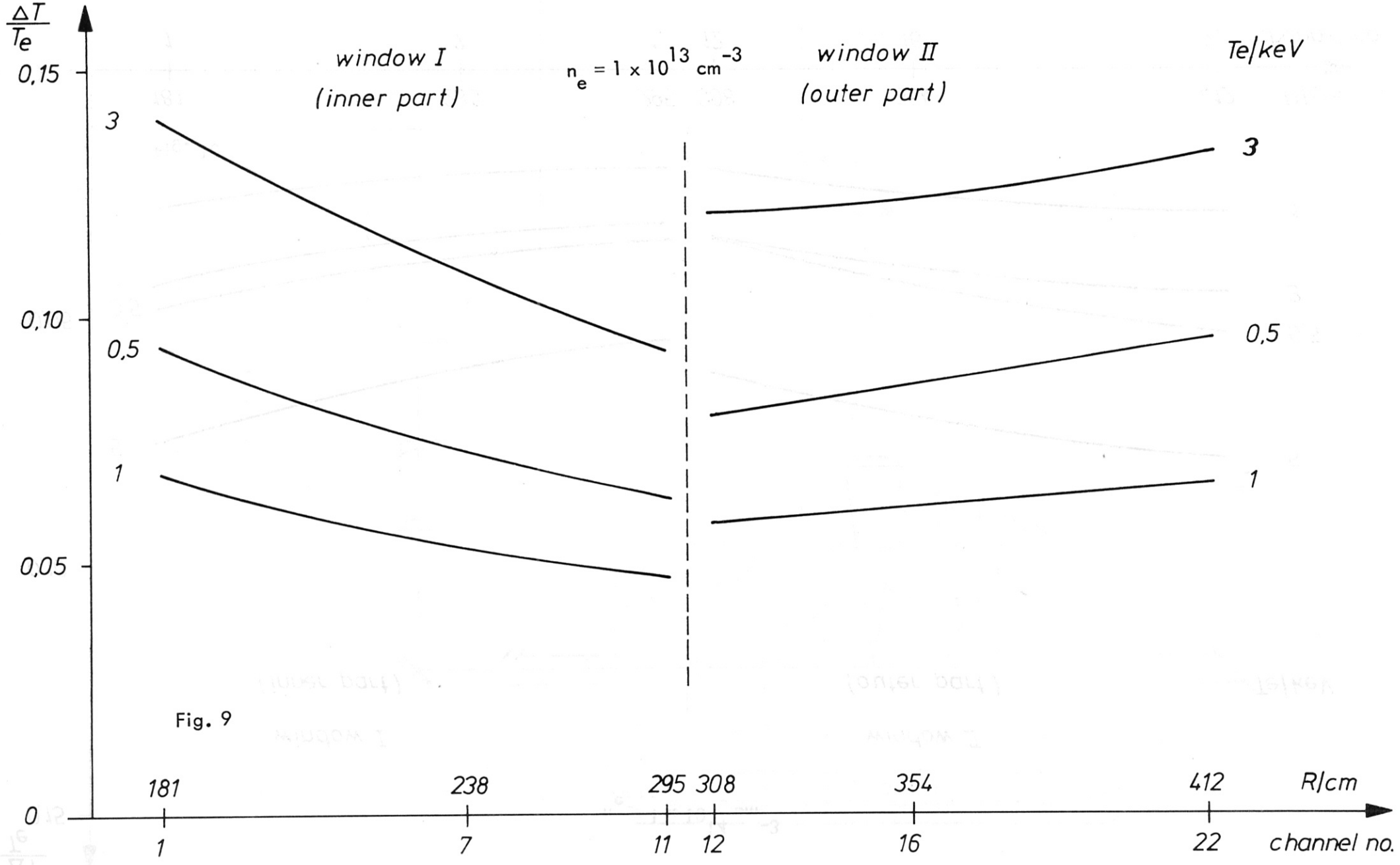
ΔT/Te
0,15
0,10
0,05
0
window I
(inner part)
n_e = 1 x 10^13 cm^-3
window II
(outer part)
Te/keV
3
0,5
1
3
0,5
1
181
238
295
308
354
412
R/cm
1
7
11
12
16
22
channel no.

Fig. 9

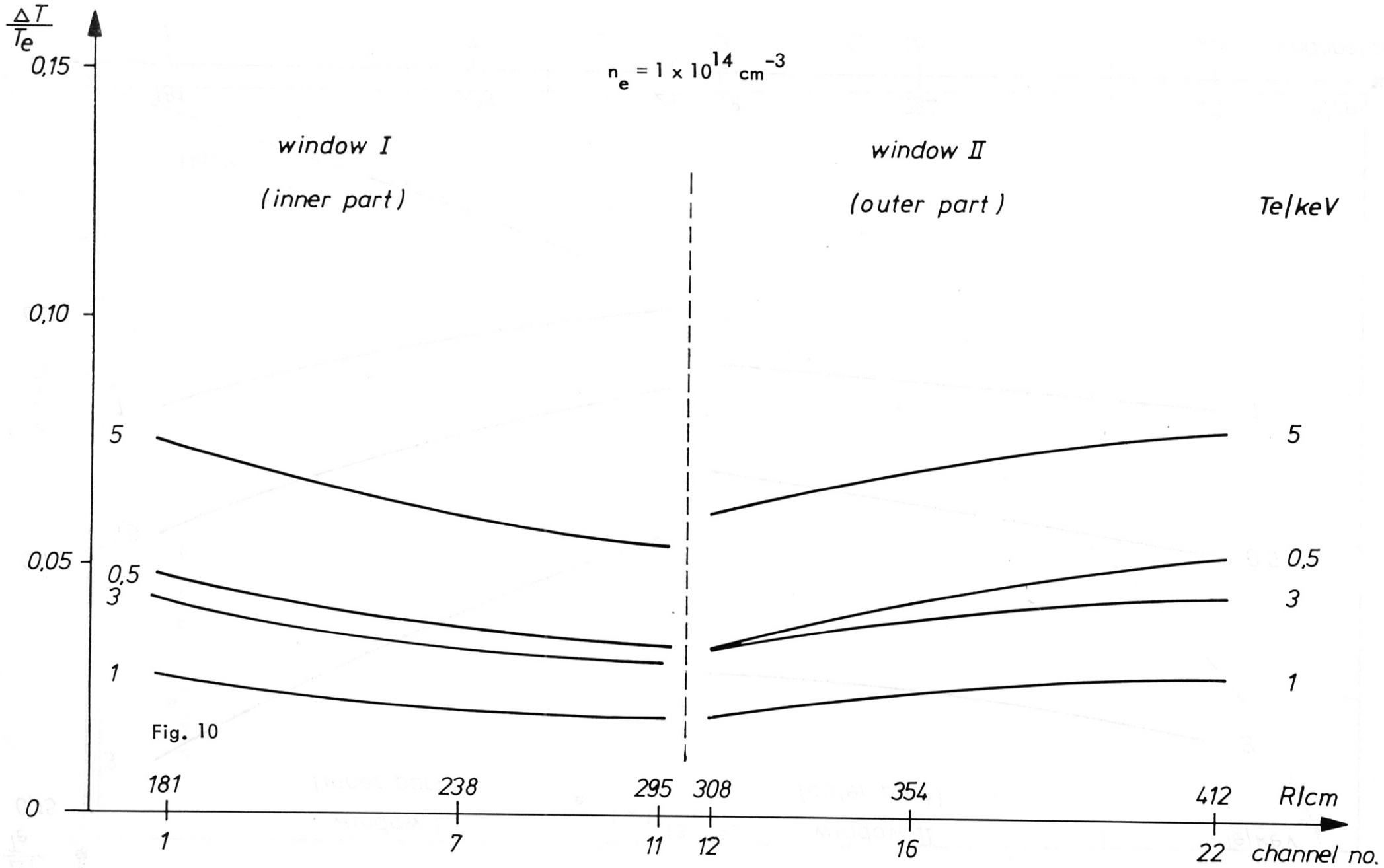
ΔT/Te
0,15
0,10
0,05
0
$n_e = 1 \times 10^{14}\ cm^{-3}$
window I
(inner part)
window II
(outer part)
Te/keV
5
0,5
3
1
5
0,5
3
1
181
238
295
308
354
412
R/cm
1
7
11
12
16
22
channel no.

Fig. 10

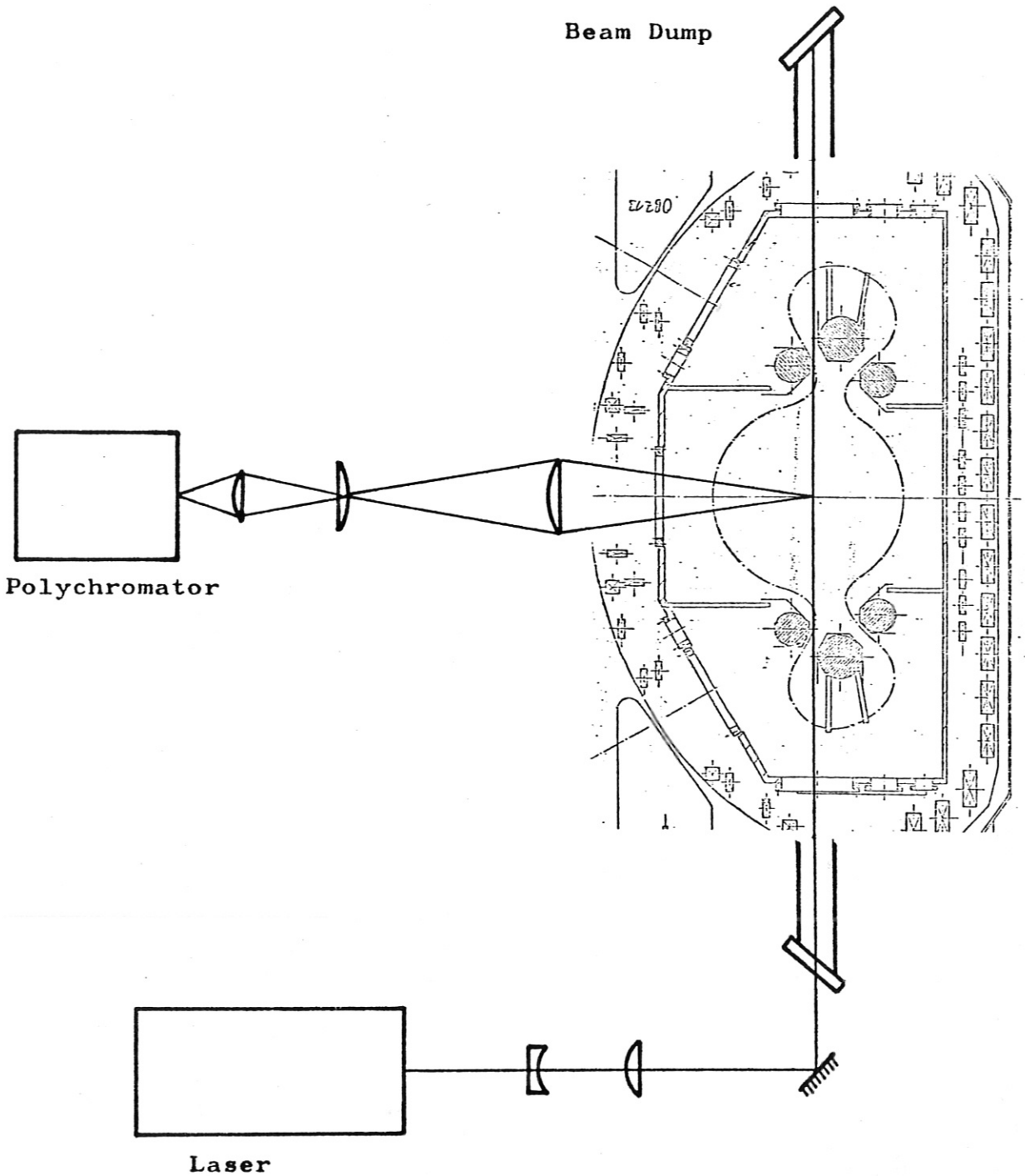

Fig. 11

With Plasma

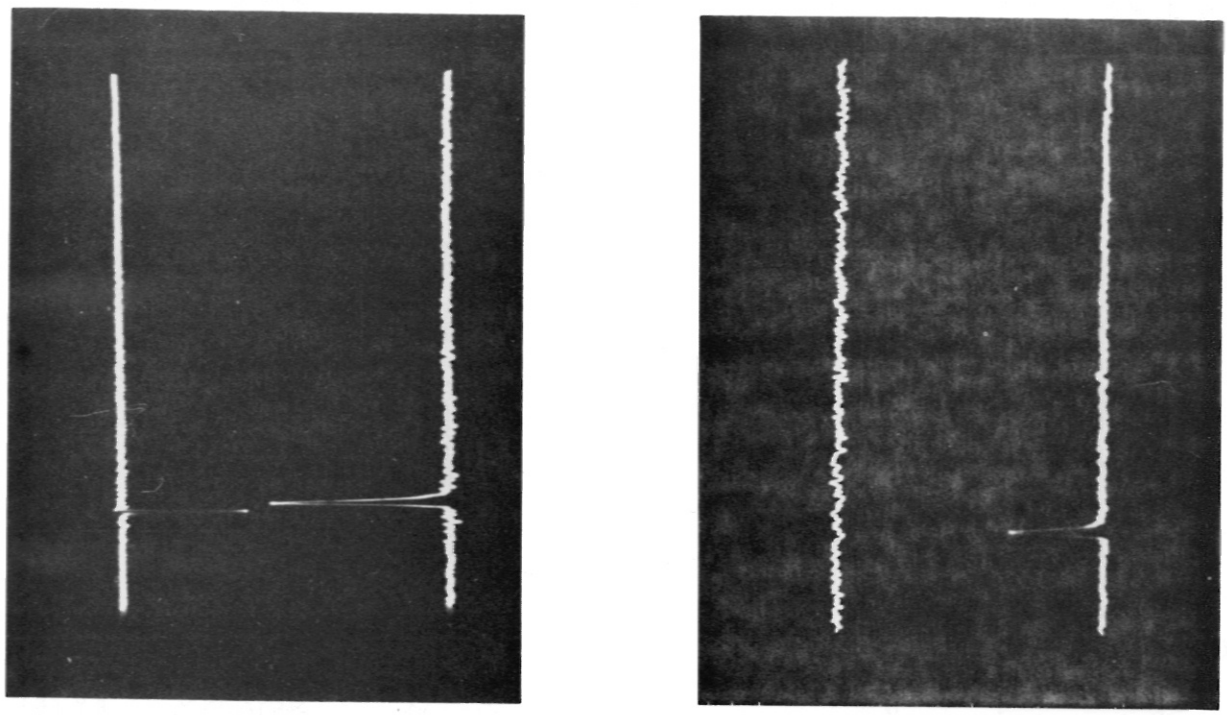

Without Plasma

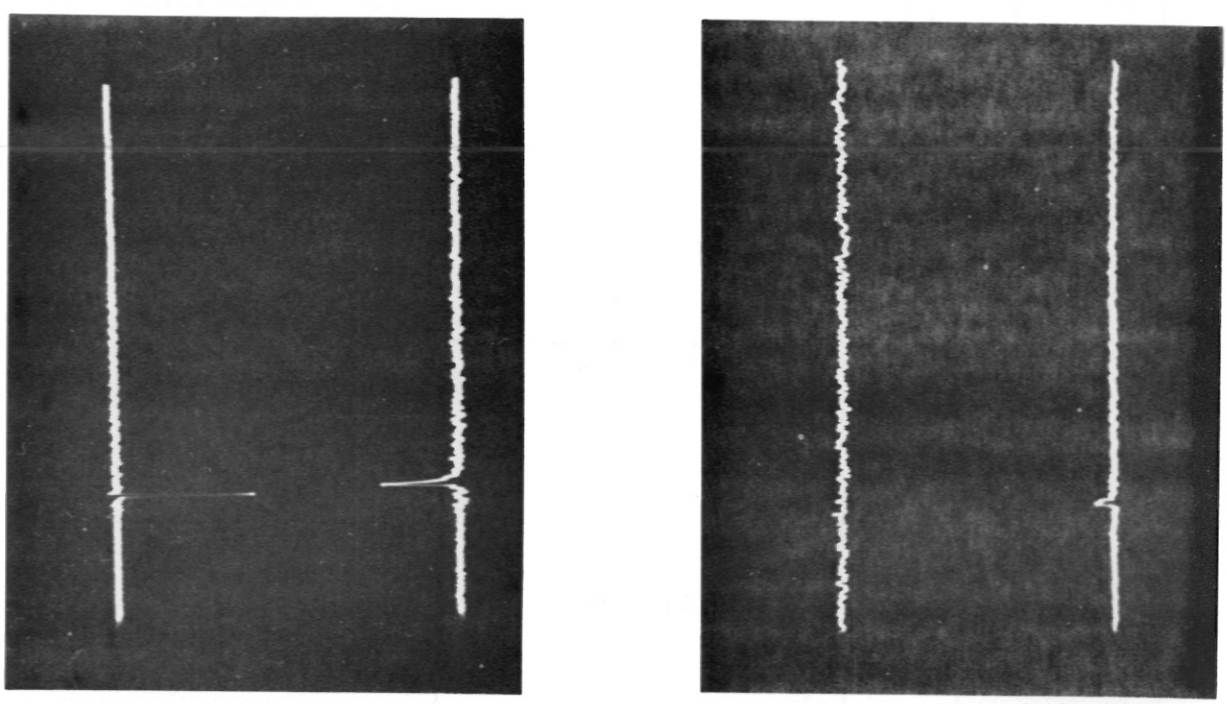

Fig.12

FIBERGUIDE INDUSTRIES

119 PARK AVENUE • SUMMIT, NEW JERSEY 07901 • (201) 522-1877

MODEL BSSSE-A

High Efficiency Low Loss Coherent Bundle

Model BSSSE-A* Bundle is constructed of specially designed SUPERGUIDE-3™ or ANHYDROGUIDE-2™ fibers depending on customer needs. The cross sectional dimensions and length are customer specified. The cross-sectional dimension is usually maintained axially for ~ 2cm. The fibers are designed to have a core-fiber area ratio of ≥ 80%. The fibers are approximately close packed at the bundle ends so that the bundle efficiency is > 60%. Price is determined on a per job basis as it is a function of the fiber cost (which depends on bundle volume) and construction time (which depends on bundle cross sectional area). Fiber cost follows the enclosed price list. Bundles are coherent to maximize information transfer, however, for most cross sections, the fiber diameter is too large for image transmission.

SPECIFICATIONS

Loss 15dB/Km @ .63μ

Efficiency > 60% @ f/2 or smaller cone optics

Length 0 to 10M (longer if possible)

Typical Cross Section: 12.5mm X 3mm

Radiation Resistant: Made of synthetic silica & high purity silicone

End Preparation: Flat & polished

Example of use: Fusion Research (Multichannel Thomson Scattering Apparatus)

* A is customer job identification number

RCA Electro Optics and Devices

data sheet no 2

Photodiode
Developmental Types

MODIFIED

C30950E, C30950F, C30950G

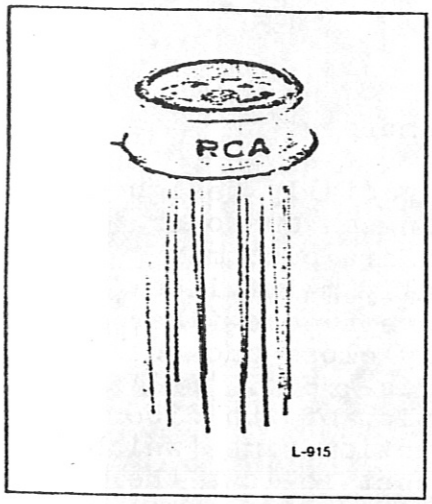

Very Wide Bandpass Silicon Avalanche Photodiode - Preamplifier Modules

- Responsivity at T_A = 25° C –
  5.6×10^5 V/W at 900 nm [50 MHz]
  1.9×10^5 V/W at 830 nm [100 MHz]
  4.9×10^4 V/W at 830 nm [200 MHz]
- System Noise Equivalent Power [NEP] at T_A = 25° C –
  2.7×10^{-14} W/Hz$^{1/2}$ at 900 nm [50 MHz]
  7.9×10^{-14} W/Hz$^{1/2}$ at 830 nm [100 MHz]
  2.6×10^{-13} W/Hz$^{1/2}$ at 830 nm [200 MHz]
- Spectral Response Range [10% Points] – 400 to 1000 nm, 400 to 1100 nm
- System Bandwidth [3 dB Point] – DC to 50 MHz, 100 MHz, 200 MHz
- Low Power Consumption
- Wide Range of Amplifier Operating Voltages
- Hermetically-Sealed Modified TO-8 Packages

RCA Developmental Types C30950E, C30950F, and C30950G are Silicon Avalanche Photodiodes with a hybrid preamplifier supplied in a single modified 12-lead TO-8 package.

The avalanche photodiode used in these devices is made using a "reach-through" structure which provides very good response between 400 and 1100 nanometers and very fast rise and fall times at all wavelengths. The preamplifier section is designed to neutralize the input capacitance of a unity voltage gain amplifier. An emitter follower is used as an output buffer stage.

To obtain the wideband characteristics, the output of these devices should be AC (capacitively) coupled to a 50-ohm termination. The module must not be DC coupled to loads of less than 10,000 ohms.

Maximum and Minimum Ratings, Absolute-Maximum Values

Photodiode Bias Voltage:			
At T_A = +70° C	600	max.	V
At T_A = -40° C	300	max.	V
Photodiode Total Current (All temp.)			
Average	100	max.	μA
Peak	100	max.	mA
Preamplifier Voltage	± 12.5	max.	V
	± 5.5	min.	V
Incident Radiant Flux, Φ_M:			
Average value	1.3	max.	μW
Peak value	1.3	max.	mW
Ambient Temperature:			
Storage, T_{stg}	-50 to +100		°C
Operating, T_A	-40 to +70		°C

Mechanical Characteristics

Type	Diode Chip (Dia.)
C30950E	C30817 (0.8 mm)
C30950F	C30902E (0.5 mm)
C30950G	C30902E (0.5 mm)

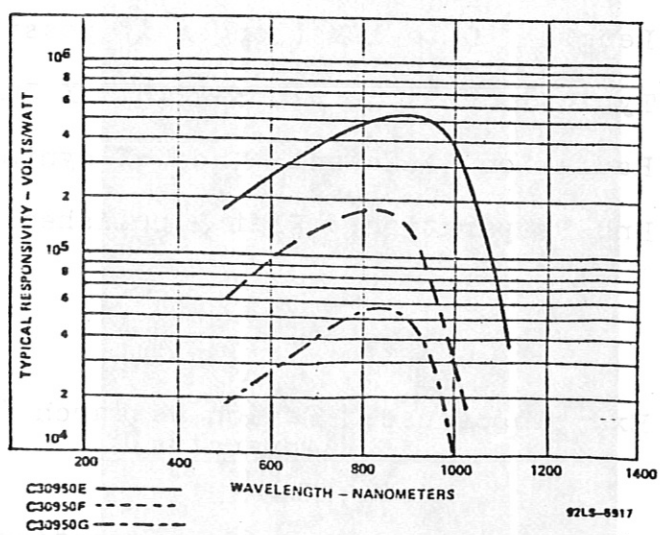

Figure 1 - Typical Spectral Responsivity Characteristics

For further information or application assistance on these devices, contact your RCA Sales Representative or Photodetector Marketing, RCA, Ste Anne de Bellevue, Quebec, Canada H9X 3L3 (514) 457-9000

Printed in U.S.A. 10-79
C30950E, C30950F, C30950G

Electrical Characteristics[1]	At an ambient temperature [T_A] of 22 °C and the DC reverse operating voltage [V_R] value supplied with each device.[2]									Units
	C30950E			C30950F			C30950G			
	Min.	Typ.	Max.	Min.	Typ.	Max.	Min.	Typ.	Max.	
Temperature Coefficient of V_R for Constant Gain[3]	-	2.2	-	-	0.6	-	-	0.6	-	V/°C
Responsivity:										
At 830 nm	4.5×10^5	5.2×10^5	-	1.7×10^5	1.9×10^5	-	5.3×10^4	5.8×10^4	-	V/W
At 900 nm	4.9×10^5	5.6×10^5	-	1.4×10^5	1.6×10^5	-	4.1×10^4	4.9×10^4	-	V/W
At 1060 nm	1.1×10^5	1.4×10^5	-	-	-	-	-	-	-	V/W
Noise Equivalent Power (NEP):										
f = 100 kHz, Δf = 1.0 Hz										
At 830 nm	-	0.029	0.057	-	0.079	0.180	-	0.260	0.570	$pW/Hz^{1/2}$
At 900 nm	-	0.027	0.060	-	0.094	0.210	-	0.310	0.730	$pW/Hz^{1/2}$
At 1060 nm	-	0.110	0.270	-	-	-	-	-	-	$pW/Hz^{1/2}$
Output Spectral Noise Voltage Density:										
f = 100 kHz – 100 MHz, Δf = 1.0 Hz	-	15	30	-	15	30	-	15	30	$nV/Hz^{1/2}$
Output Impedance	-	25	50	-	25	50	-	25	50	Ω
System Bandwidth, f_o (3 dB point)	35	50	-	70	100	-	140	200	-	MHz
Rise Time, t_r:										
λ = 900 and 1060 nm 10% to 90% points	-	7	10	-	4	5	-	2	2.5	ns
Fall Time:										
λ = 900 and 1060 nm 90% to 10% points	-	7	10	-	4	5	-	2	2.5	ns
Linear Output Voltage Swing	0.5	0.7	-	0.5	0.7	-	0.5	0.7	-	V
Voltage Swing	-	-	2.0	-	-	2.0	-	-	2.0	V
Output Offset Voltage	0.0	-0.8	-1.0	0.0	-0.8	-1.0	0.0	-0.8	-1.0	V
Supply Current	-	4.0	8.0	-	4.0	8.0	-	4.0	8.0	mA

1 All measurements are made with the device AC (capacitively) coupled into a 50 Ω termination.

2 A specific value of V_R is supplied with each device. The voltage values will be within the ranges specified below:
C30950E: 275 – 425 V
C30950F, C30950G: 180 – 250 V

3 At 830 and 900 nm.

Recommended Operating Voltage
V_R= 377 V @ 22°C
S/N 0007
Test by:
Date: 80-11-21

Pin Connections

1: Signal Output
2: No Connection, Do Not Use
3: $-V_{CC}$ Negative Bias for Amplifier
4: Positive Bias for Photodiode
5: No Connection, Do Not Use
6: Case
7: Signal Ground
8: Temp. Sensing Diode – Anode
9: Temp. Sensing Diode – Cathode
10: Ground (Power Supply)
11: No Connection, Do Not Use
12: $+V_{CC}$ Positive Bias for Amplifier

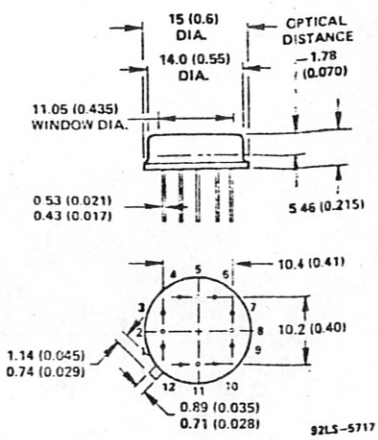

MODIFIED C30950E : C30974E

Modifications

Detector: C30974E (7mm X 1mm)

Responsivity: 3.5 x 10^5 @ 1060nm

Bandwidth: 15MHz (-3db)min.

Rise and Fall Time: 25ns max.

Dimensions in millimeters. Dimensions in parentheses are in inches.

Figure 2 – Dimensional Outline